EAST EUROPEAN JOURNAL OF PHYSICS. 3. 357-369 (2026)
DOI:10.26565/2312-4334-2026-3-31 ISSN 2312-4334

STRUCTURAL AND OPTICAL PROPERTIES OF $LiGd_{1-x}Lu_x(WO_4)_2$ Co-DOPED WITH Yb^{3+}/Er^{3+} SYNTHESIZED VIA SOLID STATE REACTION METHOD

N. Naimi[1]*, B. Rekik[1], I. Lanez[1], M. Derbal[1], L. Benharrat[2], Z. Bendaoud[1]
[1]LPCMIA Laboratory, Department of Physics, Faculty of Sciences, Saad Dahleb Blida 1 University, Blida, BP 270 Soumaa Road Blida, Algeria
[2]Research Center in Semiconductors Technology for Energy-CRTSE, 02 Bd. Dr. Frantz Fanon, B.P.140,7 Merveilles, 16038 Algiers, Algeria
**Corresponding author e-mail: phynaimi2@gmail.com*
Received January 12, 2026; revised July 17, 2026; accepted July 21, 2026

Double tungstate materials have been extensively studied and have attracted much attention as solid state lighting hosts. These materials with general formula $AB(WO_4)_2$ (A: alkali metal and B: trivalent rare earth ion) are widely used for their great optical properties. In this work, Gd^{3+}ions were partially substituted with Lu^{3+} ions to synthesize the $LiGd_{1-x}Lu_x(WO_4)_2$ compounds in order to study the structural, vibrational and optical behaviors of $LiGd_{1-x}Lu_x(WO_4)_2$ co doped with Yb^{3+} and Er^{3+} ions. Using the solid-state reaction, different concentrations of Lu^{3+} (x=2.5%, 5%, 80%, 90%, and 95%) were selected to synthesize our compounds. These concentrations influence the vibrational characteristics of the W-O bond through both band broadening and a shift in the symmetric stretching mode (ν_1). For the optical properties, green up-conversion under 980 nm excitation and down-conversion under 380 nm excitation of the double tungstate co-doped with Yb^{3+} and Er^{3+} were observed in the range of 530-552 nm. The lifetimes of the $^2H_{11/2}$ and $^4S_{3/2}$ levels, as well as the effect of Lu^{3+} substitution on the green emission of Er^{3+} in these compounds, were compared and discussed.
Keywords: *Double tungstate; Yb^{3+}/Er^{3+} co-doping; Up-conversion; Green emission*

1. INTRODUCTION

The potential applications of co-doped up-conversion (UC) materials in luminescence and sensing technologies have attracted great interest in various research fields [1-3]. Numerous studies have been devoted to rare earth co-doped up-conversion phosphors. According to the literature, Yb^{3+} and Er^{3+} ions are the most widely employed sensitizer-activator pair in up-conversion phosphors because of their favorable energy level structures, which enable efficient energy transfer processes [4-7]. In particular, the up-conversion emission of Yb^{3+} and Er^{3+} co-doped $LiGd(WO_4)_2$ double tungstate (abbreviated as LiGdW) has been extensively investigated due to its excellent luminescence properties and potential applications in several optical fields [8]. In recent years several works have been published on the co-doped mechanisms Yb^{3+}/Er^{3+} for thermometry and thermal sensing applications [9-11]. In the present work, a series of $LiGd_{1-x}Lu_x(WO_4)_2$ (x = 2.5%, 5%, 80%, 90%, and 95%) phosphors co-doped with Yb^{3+} and Er^{3+} ions were synthesized by the conventional solid-state reaction method. Comprehensive structural, vibrational, morphological, and optical characterizations were carried out using X-ray diffraction (XRD), Fourier transform infrared spectroscopy (FTIR), scanning electron microscopy (SEM), energy dispersive X ray spectroscopy (EDS), as well as Uv-vis absorption, and photoluminescence spectroscopy.

In this work, a detailed Raman spectroscopic study was performed to examine the evolution of the Raman shifts and band broadening in $LiGd_{1-x}Lu_x(WO_4)_2$ as a function of lutetium (Lu^{3+}) concentration. The results revealed a progressive structural transition from the scheelite-type $LiGd(WO_4)_2$ structure (space group $I4_{1/a}$ space group), in which Gd^{3+} and Li^+ ions occupy the same crystallographic sites and produce broader Raman bands, to the wolframite-type $LiLu(WO_4)_2$ structure (space group P_2/n), where Lu^{3+} and Li^+ ions occupy different lattice sites. Furthermore, the influence of Lu^{3+} substitution on the green up-conversion emissions of Er^{3+}, corresponding to the $^2H_{11/2}$ and $^4S_{3/2}$ to $^4I_{15/2}$ transitions, was investigated in the absence and presence of Yb^{3+} sensitizer. The fluorescence decay times of $^2H_{11/2}$ and $^2S_{3/2}$ excite states were determined for $LiGd_{1-x}Lu_x(WO_4)_2$: $1\%Yb^{3+}/0.4\%Er^{3+}$ phosphors with different Lu^{3+} contents and compared with those reported for fully substituted $LiLu(WO_4)_2$: Yb^{3+}/Er^{3+} compositions [6]. The luminescence behavior and the lifetimes associated with the intense green emissions were also estimated to assess the effect of Lu^{3+} content on the optical performance of these materials.

2. EXPERIMENTAL

2.1. Synthesis

Rare earth co-doped phosphors, $LiGd_{1-x}Lu_x(WO_4)_2$: $1\%Yb^{3+}$ /$0.4\%Er^{3+}$ (x = 2.5%, 5%, 80%, 90% and 95%) were synthesized using the solid-state reaction method. The starting materials were: Li_2CO_3 (Roth 99.999%), WO_3 (Philips, 99.97%), Gd_2O_3 (Philips, 99.99%), Lu_2O_3 (99.99%), Er_2O_3 (99.999%), and Yb_2O_3 (99.999%), all of analytical grade purity. The raw materials were weighed according to the stoichiometric molar proportions. The elaborated samples were obtained through the following chemical reaction:

$$\mathbf{Li_2CO_3 + (0.986\text{-}x)\ Gd_2O_3 + x(Lu_2O_3) + 0.004Er_2O_3 + 0.01Yb_2O_3 + 4WO_3 \rightarrow 2(LiGd_{0.986\text{-}x}Lu_{\ x}\ Er_{0,004}Yb_{0.01}(WO_4)_2) + CO_2}$$

Cite as: N. Naimi, B. Rekik, I. Lanez, M. Derbal, L. Benharrat, Z. Bendaoud, East Eur. J. Phys. 3, 357 (2026), https://doi.org/10.26565/2312-4334-2026-3-31

The prepared samples were calcined at 700°C for 14 hours, using heating and cooling rates of 5 and 10°C min^{-1}, respectively.

2.2. Characterizations

The synthesized powders obtained from the starting materials were thoroughly mixed in an agate mortar. X-ray diffraction (XRD) analysis of the $LiGd_{1-x}Lu_x(WO_4)_2$ phosphors co-doped with Yb^{3+} and Er^{3+} was performed using a Bruker-AXS D8-Discover diffractometer using Cu Anode Kα radiation (λ =1.5406 Å). The diffraction data were recorded with a step size of 0.02° in the range of 2θ from 10° to 80°. Fourier transformation infra-red (FTIR) measurements were carried out at room temperature using an FTIR-8300 spectrometer in the spectral range of 400–4000 cm^{-1}. The Raman spectra of the powders were recorded at room temperature using a Horiba Jobin-Yvon ARAMIS micro Raman spectrometer equipped with a double mono chromator and a spectrograph with holographic lattice at 1800 lines/mm. The luminescence spectra were measured under the excitation wavelengths of 380 and 980 nm using a Fluorolog- 3 spectrometer (HORIBA Jobin-Yvon). The morphology and elemental compositions of the samples were investigated by scanning electron microscopy (SEM) coupled with Energy Dispersive Spectroscopy (EDS) using a QUANTA 650 microscope equipped with a BRUKER SDD detector and an Oxford EBSD system, operating at accelerating voltage adjustable from 200 V to 30 KV.

3. RESULTS AND DISCUSSIONS

3.1. Structural properties

3.1.1. XRD of $LiGd(WO_4)_2$: x Yb^{3+} / 0.02 %Er^{3+}

Figure 1 shows the XRD patterns of LGWO: x%Yb^{3+}/2% Er^{3+} phosphors with (x= 2%,6%, and 16%). All diffraction peaks are in good agreement with the standard JCPDS card of LiGd $(WO_4)_2$phase (No: 04–008–0355). The XRD results indicate that Yb^{3+}/ Er^{3+}co-doped LGWO phosphors with x=2% and 6% are single phase materials with high crystallinity. These compounds crystallize in the scheelite structure belongs to the tetragonal system with space group $I4_{1/a}$ [12, 13]. When the Yb^{3+} concentration increases to y=16%, the single phase region transforms into a biphasic domain composed of a tetragonal scheelite $Ca(WO_4)$ phase and monoclinic (P2/n) iso-structure β-$LiYb(WO_4)_2$ [13]. With the increasing Yb^{3+} concentration, secondary Li_2WO_4 and WO_3 phases were appeared in the case of 16%Yb^{3+}/2%Er^{3+} co-doped $LiGd(WO_4)_2$. The structural parameters, including phase fractions, lattice parameters, crystallite sizes and microstrains were determined by Rietveld refinement using high score plus software. Table 1 summarizes refined structural parameters of $LiGd_{0.98-x}Yb_x$ $Er_{0.02}(WO_4)_2$ (x=2%, 6% and 16%) compounds.

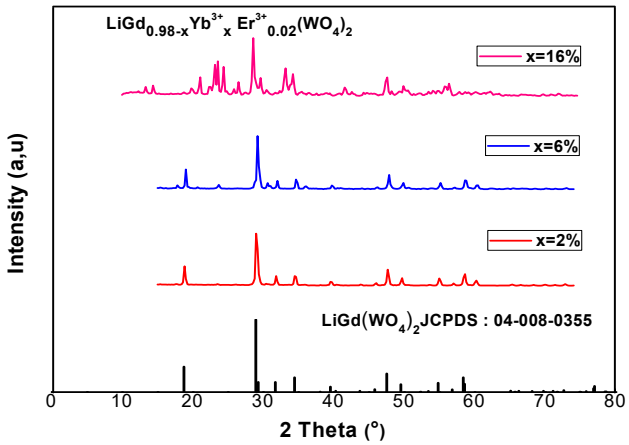

Figure 1. XRD patterns of $LiGd(WO_4)_2$: x Yb^{3+} / 2 %Er^{3+} (x=2%,6%, and 16%).

Table 1. Structural parameters of $LiGd_{0.98-x}Yb_x^{3+}$ $Er^{3+}_{0.02}$ $(WO_4)_2$ (x=2%, 6% and 16%).

$LiGd_{0.98-x}Yb_x^{3+}$ $Er^{3+}_{0.02}$ $(WO_4)_2$ (x=2%, 6% and 16%)						
Concentrations	**Weight fractions**			**Lattice parameters (A°)**	**Crystallite size (A°)**	**Micro strain (%)**
	$LiGd(WO_4)_2$	**WO_3**	**Li_2WO_4**			
2%	100%	0%	0%	a=5.195062 b=5.195062 c=11.24637 α=β=γ= 90°	453.6654	0.14554
6%	100%	0%	0%	a=5.195733 b=5.195733 c=11.25892 α=β=γ= 90°	375.685	0.6202
16%	43.8%	36%	20.3%	/	1178.345	0.09365

3.1.2. XRD of $LiGd_{1-x}Lu_x(WO_4)_2$: 1%Yb^{3+} / 0.4%Er^{3+}

Figure 2 shows the XRD patterns of $LiGd_{1-x}Lu_x(WO_4)_2$: 4%Er^{3+}, 1%Yb^{3+} phosphors with (x% =2.5%,5%,80%,90%, and 95%). The results reveal two distinct phase regions. For x ≤ 5%, the samples exhibit a scheelite-type tetragonal structure, in agreement with JCPDS card N° 04-008-0355. For higher Lu^{3+} concentrations x ≥ 80%, a phase transition from the $LiGd(WO_4)_2$ to the monoclinic $LiLu(WO_4)_2$ is observed consistent with JCPDS card No. 04-001-7757 [15], and previous reports [14,15,19]. This structural transformation is affected by the significant difference in ionic radii between Gd^{3+} and Lu^{3+} ions. The results also indicate that Lu^{3+} ions progressively substitute for Gd^{3+} ions at the cationic sites. Since Lu^{3+}, Gd^{3+}, and Er^{3+} have the same valence state (+3), and because the ionic radii of Lu^{3+}, Yb^{3+}, and Er^{3+} are very similar, the low concentrations of Yb^{3+} and Er^{3+} dopants do not induce any additional structural modifications compared with the undoped compounds reported previously [19]. With increasing Lu^{3+} concentration, a secondary Li_2WO_4 phase was appeared in the $LiGd_{1-x}Lu_x(WO^4)_2$. Table 2 summarizes the structural parameters of $LiGd_{1-x}Lu_x(WO_4)_2$: 1%Yb^{3+} / 0.4%Er^{3+} (x%=2.5%,5% ,80%, 90%, and 95%).

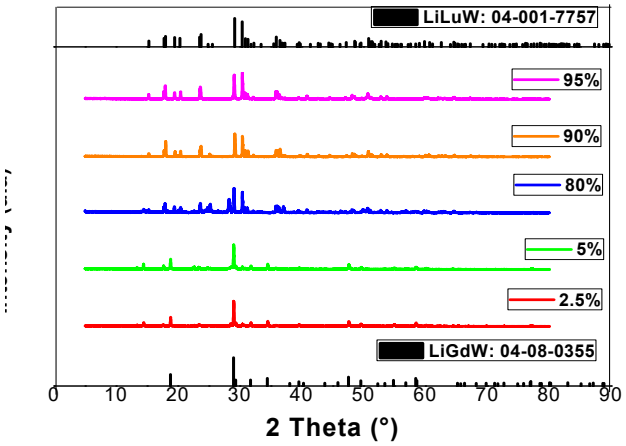

Figure 2. XRD patterns of $LiGd_{1-x}Lu_x(WO_4)_2$: 1%Yb^{3+} / 0.4%Er^{3+} (x%=2.5%,5% ,80%, 90%, and 95%).

Table 2. Structural parameters of $LiGd_{1-x}Lu_x(WO_4)_2$: 1%Yb^{3+} / 0.4%Er^{3+} (x%=2.5%,5% ,80%, 90%, and 95%).

$LiGd_{1-x}Lu_x(WO_4)_2$: 1%Yb^{3+} / 0.4% Er^{3+}						
Concentrations	**Weight fractions**			**Lattice parameters (A°) and angles (°)**	**Crystallite sizes (A°)**	**Micro strain (%)**
	$LiGd(WO_4)_2$	$LiLu(WO_4)_2$	Li_2WO_4			
x=2.5%	81.6%	17.3%	1.2%	a=5.1967 b =5.1967 c = 11.254 α=β=γ= 90°	370.1438	0.31012
x=5%	78.4%	21.2%	0.3%	a=5.1937 b=5.1937 c=11.244 α=β=γ= 90°	1215.532	0.09359
x=80%	1.2%	94%	4.8%	a =4.9914 b =5.7982 c =10.817 α=β= 90° γ= 113.934°	1805.904	0.04949
x=90%	0.1%	98%	1.8%	a = 4.9854 b = 5.7937 c = 10.7989 α=β= 90° γ= 114.307°	1912.459	0.06543
x=95%	0.8%	99.2%	0%	a =4.9911 b =5.7970 c =10.8141 α=β= 90° γ= 113.998°	1052.2	0.11905

3.1.3. XRD of $LiLu(WO_4)_2$: xEr^{3+}, and $LiLu(WO_4)_2$: xYb^{3+} / 2% Er^{3+}

Figure 3 shows the XRD patterns of $LiLu_{1-x}(WO_4)_2$: xEr^{3+} (x=0.1%,0.2% ,2%) and the $LiLu_{1-x-y}(WO_4)_2$ with (x = 2%, 6%, 16%; y =2%). All diffraction peaks can be well indexed to the standard pattern of pure $LiLu(WO_4)_2$ (JCPDS No.04-001-7757), indicating that the incorporation of Yb^{3+} and Er^{3+} ions does not alter the crystal structure of the host

matrix, even at a high Yb^{3+} concentration of 16%. This behavior changes from that observed in $LiGd(WO_4)_2$ and can be attributed to the fact that $LiLu(WO_4)_2$ and $LiYb(WO_4)_2$ share the same monoclinic β-$LiYb(WO_4)_2$. All the compounds crystallize in monoclinic system with the space group of $P_{2/n}$ [11]. The crystal structure is composed of interconnected [LiO_6], [LuO_6], and [WO_6] octahedra. For a coordination number (CN) of six, the ionic radii of Li^+, Lu^{3+}, W^{6+}, Yb^{3+} and Er^{3+} ions are 0.76 Å, 0.861 Å, 0.60 Å, 0.86 Å and 0.89 Å, respectively. The structural parameters obtained from Rietveld refinement for $LiLu(WO_4)_2$: xEr^{3+} (x=0. 1%,0.2%, and 2%)) and $LiLu(WO_4)_2$: xYb^{3+} / 2% Er^{3+} (y =2%,6%, and 16%) are summarized in table 3.

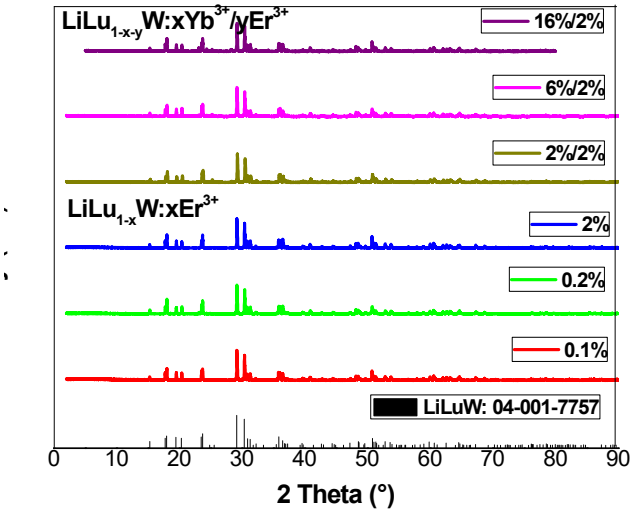

Figure 3. XRD patterns of $LiLu(WO_4)_2$: xEr^{3+} (x=0.1%,0.2%, and 2%)) and $LiLu(WO_4)_2$: xYb^{3+} / 2% Er^{3+} (y =2%,6%, and 16%)

Table 3. Structural parameters of $LiLu(WO_4)_2$: xEr^{3+} (x=0.1%,0.2%, and 2%)) and $LiLu(WO_4)_2$: xYb^{3+} / 2% Er^{3+} (y =2%,6%, and 16%).

$LiLu(WO_4)_2$: xEr^{3+} (x=0.1%,0.2%, and 2%))				
Concentrations	**Weight fractions** $LiLu(WO_4)_2$	**Lattice parameters (A°) and angles (°)**	**Crystallite sizes (A°)**	**Micro strain (%)**
x=0.1%	100%	a=4.98398 b=5.79410 c=10.79730 α=γ= 90° β= 114.3644°	2278.823	0.0349
x=0.2%	100%	a=4.98670 b=5.79105 c=10.79680 α=γ= 90° β= 114.303°	3780.809	0.02541
x=2%	100%	a=4.98375 b=5.79427 c=10.79762 α=γ= 90° β= 114.3670°	13831.33	0.00626
$LiLu(WO_4)_2$: xYb^{3+} / 2% Er^{3+} (y =2%, 6%, and 16%)				
x=2% y=2%	100%	a=4.98640 b=5.79310 c=10.79800 α=γ= 90° β= 114.320°	3299.103	0.0296
x=2% y=6%	100%	a=4.9858 b=5.7916 c=10.7963 α=γ= 90° β= 114.3073°	3273.314	0.02642
x=2% y=16%	100%	a=4.98413 b=5.79340 c=10.7970 α=γ= 90° β= 114.3432°	4058.184	0.01574

Figure 4 (a) and 4 (b) show the SEM image of x%Yb^{3+}/2%Er^{3+} co-doped LGW (x=2 and 6) samples, respectively. The micrographs reveal that the synthesized samples exhibit relatively smooth surfaces with slight agglomeration. The

particle sizes are in the of micrometer range. The observed compact and morphology is favorable for obtaining strong up-conversion luminescence, as reported in reference [8], this morphological result indicates that this compound appears to be a promising candidate for UC luminescence. To evaluate the elemental composition, EDS analysis was carried out. Figure 4(c) shows the EDS results of LGWO: x%Yb^{3+}/ 2% Er^{3+} (y=2%, 6%, and 16%), confirming the presence of all constituent element: gadolinium, ytterbium, erbium and tungsten.

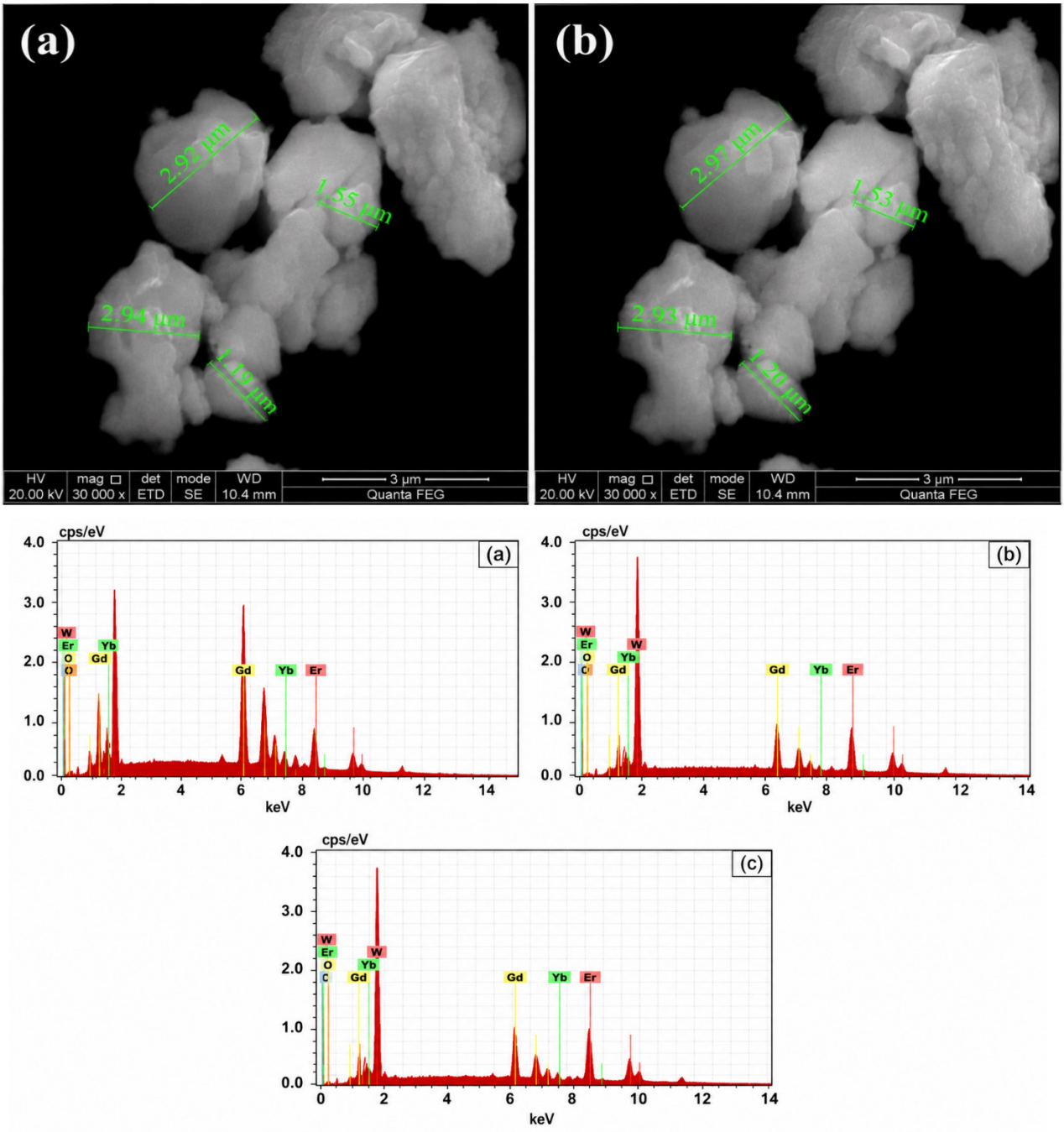

Figure 4. (a) SEM image of LiGdWO: 2% Yb^{3+}/2% Er^{3+}, (b) SEM image of LiGdWO: 6% Yb^{3+}/2% Er^{3+}, and (c) EDS analysis of LGWO: x%Yb^{3+}/ 2% Er^{3+}(x=2%, 6%, and 16%)

3.2. Vibrational properties

3.2.1. FTIR analysis

The FTIR spectra of $LiGd_{1-x}Lu_x(WO_4)_2$ and $LiGd_{1-x}Lu_x(WO_4)_2$: 1%Yb^{3+}/0.4%Er^{3+} with (x=2.5%, 5%, 80%, 90%, and 95%) were recorded at room temperature (Fig. 5). For x = 2.5% and 5%, the spectra are similar to those of the prototype scheelite structure. The assignment of the IR vibrational frequencies is in good agreement with previous reports [17-19]. The isolated tetrahedral (WO_4) groups exhibit four fundamental vibrational modes, which can be classified into two categories corresponding to the stretching and bending modes of vibrations. Each category is further divided into symmetric and asymmetric modes. The most intense band located at 915 cm^{-1}, is attributed to the symmetric stretching

vibration of the (WO_4) tetrahedra, whereas the bands observed in the 700-850 cm^{-1} region correspond to the asymmetric stretching modes. Co-doping with 2%Er^{3+}, 2% Yb^{3+} and 6% Yb^3 does not significantly modify the vibrational modes. This behavior can be attributed to the conservation of the scheelite structure at relatively low dopant concentrations.

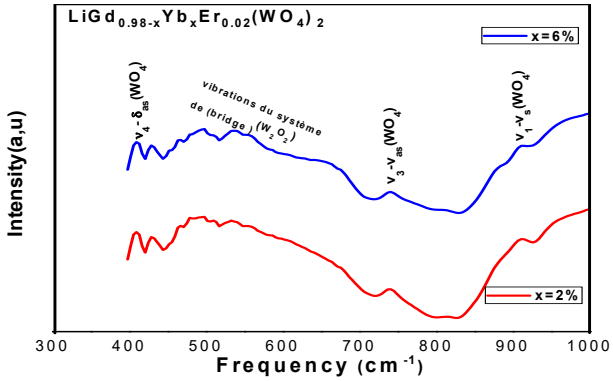

Figure 5. FTIR spectra of $LiGd_{0.986-x}Yb_xEr_{0.02}(WO_4)_2$ with (x =2 % and 6%)

For x = 80%, 90%, and 95%. FTIR spectra shown in Figure 6 present vibrational modes characteristic of the wolframite structure. The internal modes observed at 500.28 cm^{-1}, 553.39 cm^{-1}, 672.09 cm^{-1}, 790.79 cm^{-1} can be assigned to the asymmetric stretching mode υ_{as} (WO_6). In contrast, no absorption bands were detected in the interval 500 cm^{-1} to 800 cm^{-1} for x= 2.5%, 5% (LGW phase). The appearance of these bands for x≥80%, corresponding to the LLuW phase, confirms the structural transition from the scheelite to the wolframite phase [20].

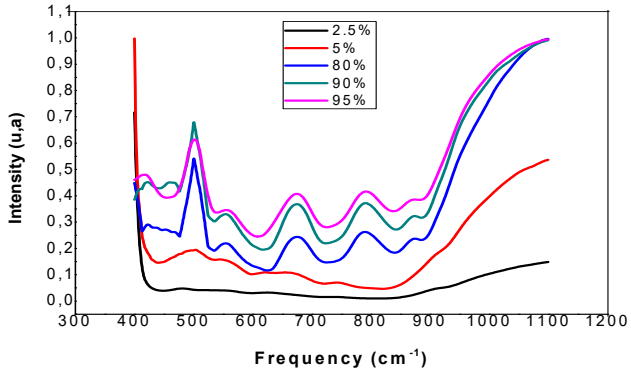

Figure 6. FTIR spectra of $LiGd_{1-x}Lu_xW$ with: x=2.5%, 5%, 80%, 90%, and 95%.

3.2.2. Raman study

Figure 7 presents Raman spectra in the frequency range of 50-1000 cm^{-1} at room temperature for the $LiGd_{1-x}Lu_x(WO_4)_2$ sample co-doped with 1% Yb^{3+} and 0.4% Er^{3+} for x=2.5, 5, 80, 90 and 95%.

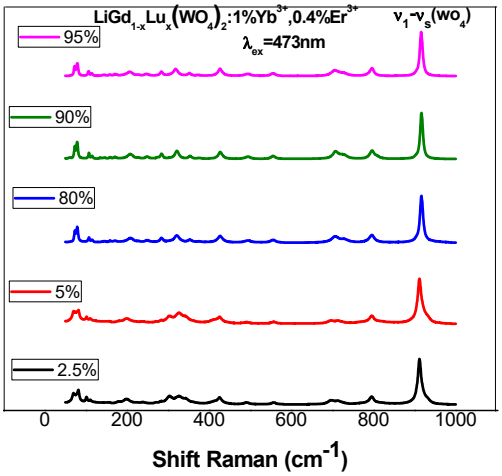

Figure 7. Raman spectra of $LiGd_{1-x}Lu_x$ $(WO_4)_2$:1%Yb^{3+}/0.4%$Er^{3+}$with different Lu^{3+} concentrations

These results exhibit vibration peaks of internal modes extending from 200 to 920 cm^{-1} with four fundamental vibrations corresponding to the stretching mode at (ν_1=913cm^{-1}), (ν_3=833cm^{-1}), and binding mode at (ν_2=320cm^{-1}), (ν_4=405cm^{-1}) of the WO_4^{2-} ions, while the external vibration region is located below 200 cm^{-1}. The vibrational characteristics in the internal-mode region demonstrate full agreement between the structure and its phonon properties.

The vibrational frequencies are summarized in Table 4. The distinct gap in the region of 420-740 cm^{-1} in the energy distribution of K=0 phonons is clearly shown in the spectra of the compounds under study for x = 2.5 and 5% being iso structural to $Ca(WO_4)$, which crystallizes in the scheelite type with tetragonal system and space group $C_{4h}^6 = I4_1/a$, the coordination numbers of the scheelite structure are characterized by CN (Li^+) = 8, CN (Gd^{3+}) = 8, the same position with site symmetry (SS) =C_2 occupied by both Li^+ and Gd^{3+}. With increasing Lu^{3+} concentration, new peak appears at 153, 207, and 248 cm^{-1}, indicating the doubled of line's number for the monoclinic phase, due to the splitting of pertinent bands and arising of additional bands in the energy gap region due to the intermolecular interaction in the wolframite- type unit cell that the isolated WO_4^{-2} units tungsten ions coordinated to four oxygen CN (W^{6+}) = 4, occupy the S_4 symmetry [20].

Table 4. Vibration modes of $LiGd_{1-x}Lu_xW$ x=2.5%, 5%, 80%, 90%, and 95%.

Frequency (cm^{-1}) **Present work**	Frequency (cm^{-1}) [14]	IR vibration modes	Frequency (cm^{-1}) **Present work**	Frequency (cm^{-1}) [14]	Raman vibration modes
81.05	81.05	T(Gd^{3+}) and T (W_2O_8)	79.50	76.60 95.40 100.07	T(Gd^{3+})-T(W^{6+})
			109.8	106.90 143.58	T(Gd^{3+})-T(W^{6+})
528	500.28 553.39	υ 4 -υ as WO_4	153.8	167.04 170.45 187.52	T(Gd^{3+}) and T(W_2O_8)
			207.57	200.74 207.57	υ 2-&s WO_4 T(Li^+)
			248.09	237.85 237.85	υ 2-&s WO_4 T(Li^+)
672.09	672.09 790.79	υ 3 -υ as WO_4	285.21	305.26 268.147	&s bending modes T(Li^+)
			321.89	328.72 305.26	&s bending modes T(Li^+)
			355.59	429.82 369.24 359.01	&s bending modes
			493.8	490.40 416.17	υ 4- &s WO_4
			557.37	507.37 507.37 608.14	υ as stretching mode
			708.81	702.41 722.46	υ as stretching mode
			796.26	796.26 769.39 779.13 820.15 856.84	υ 3-υasWO_4
			917	911.02 907.05	υ 1- υ s WO_4

There is a relationship between Raman shift of the highest energy peak ($\nu_{1=}$ vs = 913cm^{-1} (Stretching symmetric peak)) and Lu^{3+} concentrations which it shift toward a higher wave number values (Fig. 8), indicate that it corresponds to ionic radius size, as the Gd^{3+} (1.053 Å) substitution by Lu^{3+} (0.861 Å) in the compound decrease the average ionic radii size ($R_{average} = R_{Lu}$ x+ R_{Gd} (1-x)), For better explain, this symmetric stretching peak vs give more information of W—O links behavior, that is more sensible to cationic environmental variation and is strongly influence by the Ln-O-W, with Ln=Lu/Gd, which introduce covalence evolution of this bond.

On the other hand, the result presented in Figure 8 shows clearly that the band width of the stretching symmetric peak (strongest peak) of the tetragonal structure of LGW is larger than that of the monoclinic structure corresponding to LLuW. It well knows the broadening of vibrational bands in Raman spectra provides information on structural disorder because wide vibration bands are a well-known characteristic of irregular systems [14], which is directly proportional to the Raman gain, and it can be used as a condition for comparing the performance of the studied materials [21]. To explain this phenomenon, we calculate the ratio of the Raman intensity to the full width at half maximum (FWHM) [21]. This parameter is estimated by the following relationship (1) [21]:

$$\sum = I/W \quad (1)$$

which I: the intensity, and W= ω: Full-Width for the Half-Maximum (FWHM).

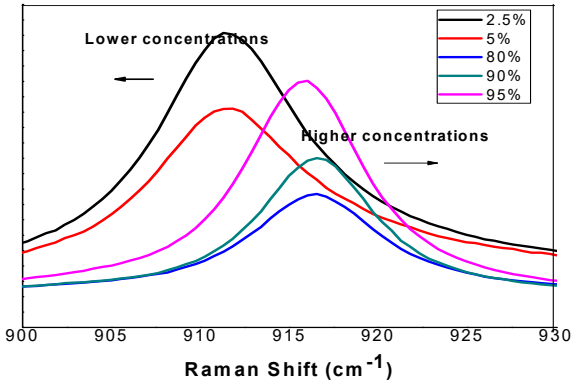

Figure 8. Expanded view of the strongest Raman band of $LiGd_{1-x}Lu_x(WO_4)_2$ at different Lu^{3+}concentrations.

The Raman spectra were fitted using a Lorentzian function to determine the peak intensity ''I'' and FWHM =W. Table 5 summarizes the parameters of the strongest symmetric stretching mode (ν). ∑= I/W ratio was used to evaluate the degree of structural disorder. The results show that samples with low Lu^{3+} concentrations crystallize in the scheelite structure, while the wolframite phase is appeared with higher concentration of Lu^{3+}.
Lorentz function

$$y = y_0 + \frac{2A}{\pi}\frac{\omega}{4(X-X_C)^2+\omega^2} \quad (2)$$

$$I = 2A/\pi\omega \quad (3)$$

$$\omega = W \quad (4)$$

Table 5. Experimental frequencies and Raman active phonon position bands, and comparison between ∑ Raman shift of $LiGd_{1-x}Lu_x(WO_4)_{2x}$= 2.5%, 5% ,80%, 90%, and 95%

Component	Function type	W, (cm^{-1})	A, (u.a).cm^{-1}	I, (u.a)	ω, (cm^{-1})	∑ ratio
x=2.5 %	Lorentz	11.68	204081.67	11123.38	11.68	951.80
x=5 %	Lorentz	10.44	262515.47	16003.60	10.44	1531.75
X=80%	Lorentz	8.32	84264.62	6446.28	8.32	774.23
x= 90 %	Lorentz	7.04	98617.78	8911.03	7.04	1264.15
x= 95 %	Lorentz	7.39	161329.813	13899.34	7.39	1880.06

A simple interpretation of these results can be proposed by considering that the smaller the cation Ln^{3+}, the greater its interaction with the electron cloud of its neighboring oxygen's will be and the greater degree of covalence of the bonds forms with the latter. The covalent bond is by its nature; directional, unlike the ionic bond. This will therefore have the consequence of slowing down and limiting the movements of the oxygen's involved, around their equilibrium position, if their movement is limited with respect to the trivalent Ln cation, it will also be limited with respect to W, thus leading to a rigidity of the W— O bonds as shown in Figure 9.

(a) (b)

Figure 9. Influence of Ln (L) size on the nature of Ln-O, (a): completely covalent bonding, and (b) partially ionic bonding

This phenomenon will then induce an increase in the force constants of these which is naturally reflected in vibrational spectroscopy by an increase in the vibration frequency of these bonds that indicate the W—O peak shift toward the higher wave number values [20-21].

3.3 Optical properties

3.3.1. Absorption spectra

Figure 10 and 11 present the room temperature absorption spectra at of $LiGd(WO_4)_2$: x% Yb^{3+}/ 2% Er^{3+} phosphors. For x=0, several absorption peaks are observed at 348.55, 383.66, 454.59, 489.11, 526.35, 635.74 and 977.32 nm corresponding to the Er^{3+} transitions from the ground state $^4I_{15/2}$ to the excited states $^4G_{11/2}$,$^4F_{3/2}$, $^4F_{7/2}$, $^4S_{3/2}$,$^2H_{11/2}$,$^4F_{9/2}$, $^4I_{11/2}$ respectively. For x= 2 % and 6%, figure 11 reveals two charge-transfer bands (CTBs) located at approximately

233 nm and 267 nm, which assigned to the W^{+6}-O^{-2} and Yb^{+3}-O^{-2} charge transfer transitions, respectively. The W-O CTB is more intense for x=2% than for x=6%, which may be related to the enhanced absorption by Yb^{3+} ions. This behavior suggests that the broad band around 267 nm originates from the presence of Yb^{3+} ions and can therefore be attributed to the O^- toYb^{3+} charge transfer transition. In addition, all samples exhibit a broad absorption band around 980 nm. The large bandwidth in this region is attributed to the overlap of the Yb^{3+} ($^2F_{7/2}\rightarrow{}^2F_{5/2}$) and Er^{3+} ($^4I_{15/2}\rightarrow{}^2H_{11/2}$) absorption transitions.

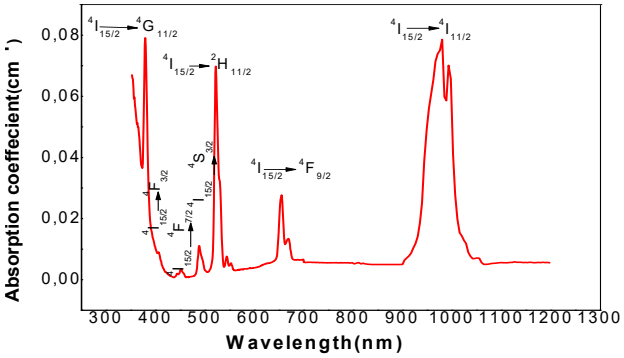

Figure 10. Absorption spectra of LiGd $(WO_4)_2$: 2% Yb^{3+}/ 2% Er^{3+}

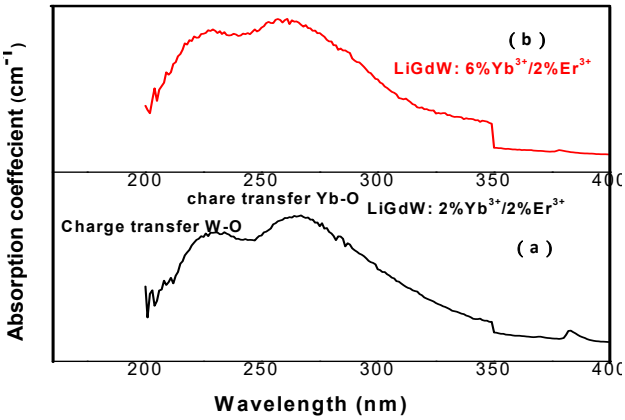

Figure 11. (a) Absorption spectra of LiGd $(WO_4)_2$: 2% Yb^{3+}/2% Er^{3+}, **(b)** Absorption spectra of LiGd $(WO_4)_2$: 6% Yb^{3+}/2% Er^{3+}

3.3.2. Excitation spectrum

Figure 12 shows the excitation spectrum of $LiGd(WO_4)_2xYb^{3+}2\%\ Er^{3+}$ (x=2% and 6%) recorded at room temperature by monitoring the emission at λ_{em}= 550 nm in the 200 and 450 nm wavelength range. The spectra exhibit a strong excitation peak centered at 380 nm, which assigned to the $^4I_{15/2} \rightarrow {}^4G_{11/2}$ transition of Er^{3+}. This result confirms the presence of the same transition observed in the absorption spectra.

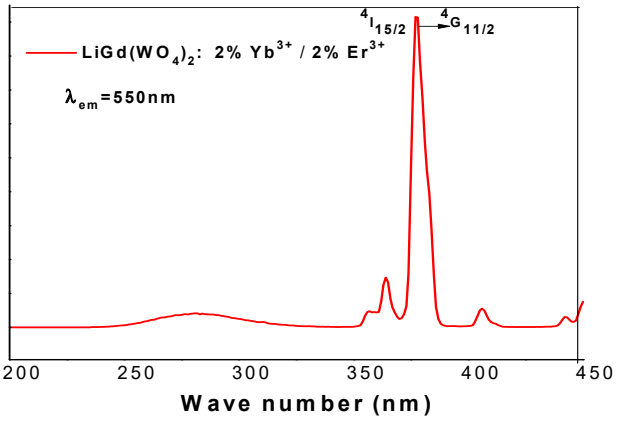

Figure 12. Excitation spectrum of LiGd $(WO_4)_2$: 2% Yb^{3+}/ 2% Er^{3+}.

3.3.3. Down-conversion emission spectra

Figure 13 shows the down-conversion emission spectra of $LiGd(WO_4)_2$: xYb^{3+}/2% Er^{3+} phosphors with x= 2%,6% and 16% under 380 nm excitation. The samples exhibit two green emission bands centered at 532 nm and 550 nm, corresponding to the ($^2H_{11/2} \rightarrow {}^4I_{15/2}$ and $^4S_{3/2}\rightarrow{}^4I_{15/2}$) transitions of Er^{3+} respectively. The intensity of the green emission strongly depends on the Yb^{3+}/Er^{3+}ratio. As the Yb^{3+} concentration increases, cross relaxation (CR) processes become more significant. In particular, the process: $Er^{3+}(^4S_{3/2})+Er^{3+}(^4I_{15/2}) \rightarrow Er^{3+}(^4I_{9/2}) + Er^{3+}(^4I_{13/2})$ partially depopulates the ($^2H_{11/2}$/ $^4S_{3/2}\rightarrow{}^4I_{15/2}$) levels, thereby reducing the probability of the green radiative ($^2H_{11/2}$/ $^4S_{3/2}\rightarrow{}^4F_{9/2}$). Instead, non-radiative relaxation pathways become dominant, leading to a decrease in the population of the $^4S_{3/2}$ level and an increase in the population of the $^4I_{13/2}$ level. At higher dopant concentrations, the down –conversion process is also influenced by phonon assisted energy transfer. The coupling process: $Er^{3+}(^4S_{3/2}) + Yb^{3+}(^2F_{7/2}) \rightarrow Er^{3+}(^4I_{9/2}) + Yb^{3+}$ ($^2F_{5/2}$), further decreases the population of the $^4S_{3/2}$ level while increasing that of the $^4I_{9/2}$ level. Subsequently, the population accumulated in the lower excited states can contribute to the population of the $^4F_{9/2}$ level. For the sample containing 16% of Yb^{3+}, no emission is observed, which is consistent with the XRD results reported previously [12], Moreover, no red emission band corresponding to the $^4F_{9/2} \rightarrow {}^4I_{13/2}$ transition of Er^{3+} is detected in the spectra. This absence of red emission indicates that the multi-phonon relaxation $^4S_{3/2}$ to $^4F_{9/2}$ is not sufficiently efficient to populate the $^4F_{9/2}$ level.

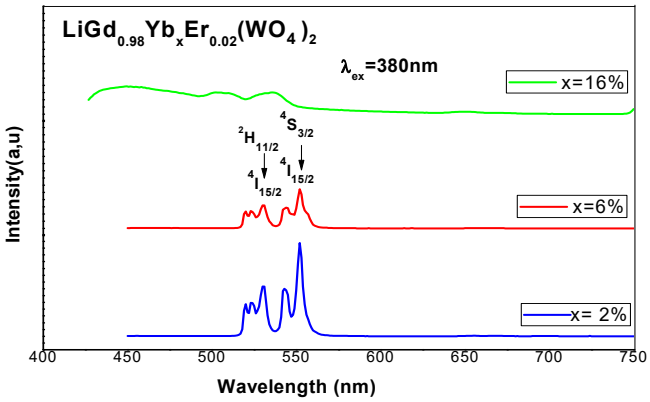

Figure 13. Down-conversion emission spectra of $LiGd(WO_4)_2$: x%Yb^{3+}/ 2%Er^{3+}, (x=2%, 6%, and 16%), excited at 380 nm

Figure 14 presents the down-conversion emission spectra of $LiGd_{1-x}Lux(WO_4)_2$: 1% Yb^{3+}/ 0.4% Er^{3+} phosphors with x= 2.5%, 5%, 80%, 90%, 95% under 380 nm excitation. For the low Lu^{3+} concentrations (x%=2.5%, and 5%), the samples exhibit two green emission bands centered at 521 nm and 541 nm, corresponding to the $^2H_{11/2} \rightarrow {}^4I_{15/2}$ and $^4S_{3/2} \rightarrow {}^4I_{15/2}$ transitions of Er^{3+} respectively. With increasing Lu^{3+} substitution (x = 80%,90%,95%), the emission bands shift slightly 523 and 543 nm, respectively. These values are comparable to those reported in the reference [16], and $LiGd(WO_4)_2$ (LGW) in reference [10,19]. Although the overall shapes of the emission bands remain unchanged, a slight red shift is observed due to the difference in ionic radii and electronegativity between Gd^{3+} and Lu^{3+} ions. These factors induce distortions in the crystal lattice, as discussed in the structural and vibrational studies.

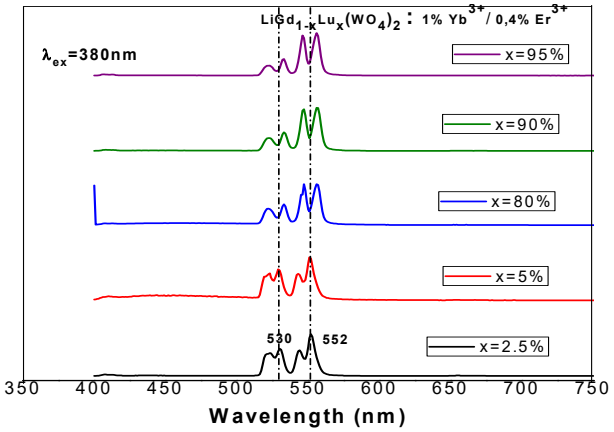

Figure 14. Down-conversion emission spectra of $LiGd_{1-x}Lu_x(WO_4)_2$: 1% Yb^{3+}/ 0.4% Er^{3+}, excited at 380 nm with x= 2.5%, 5%, 80%, 90% and 95%.

3.3.4. Up-conversion emission spectra

Figure 15 shows the up-conversion emission spectra of LiGd $(WO_4)_2$: x% Yb^{3+}/ 2 % Er^{3+} phosphors (x= 2%, 6%, 16%) under 980 nm excitation. The samples exhibit a strong green up-conversion emission bands centered at approximately 550 nm, which is attributed to $^4S_{3/2}$ to $^4I_{15/2}$ transition of Er^{3+} ions.

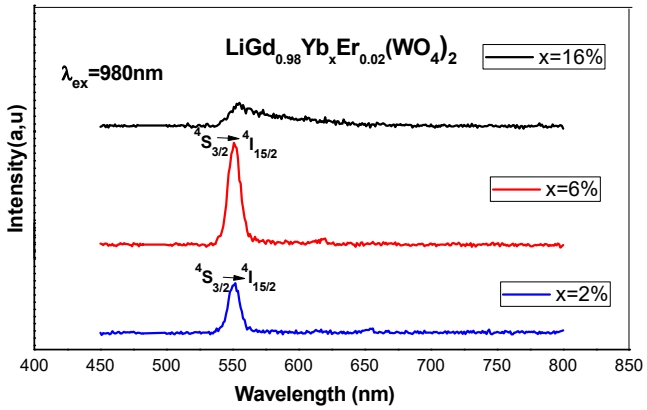

Figure 15. Up-conversion emission spectra of LiGd $(WO_4)_2$:
x% Yb^{3+}/ 0.02% Er^{3+}, (x= 2%, 6%, and 16%) excited by a 980 nm

3.3.5. Fluorescence Decay Kinetics

The fluorescence decay kinetics corresponding to the $^2H_{11/2} \rightarrow {}^4I_{15/2}$ and $^4S_{3/2} \rightarrow {}^4I_{15/2}$ transitions of Er^{3+} ions in the co-doped $LiGd_{1-x}Lu_x(WO_4)_2$ system (with x = 2.5%, 5%, 80%, 90%, and 95%) are presented in Figures 16 (a) and (b). These decays were recorded under an excitation wavelength of 380 nm, with emission monitored at 525 nm and 551 nm, respectively.

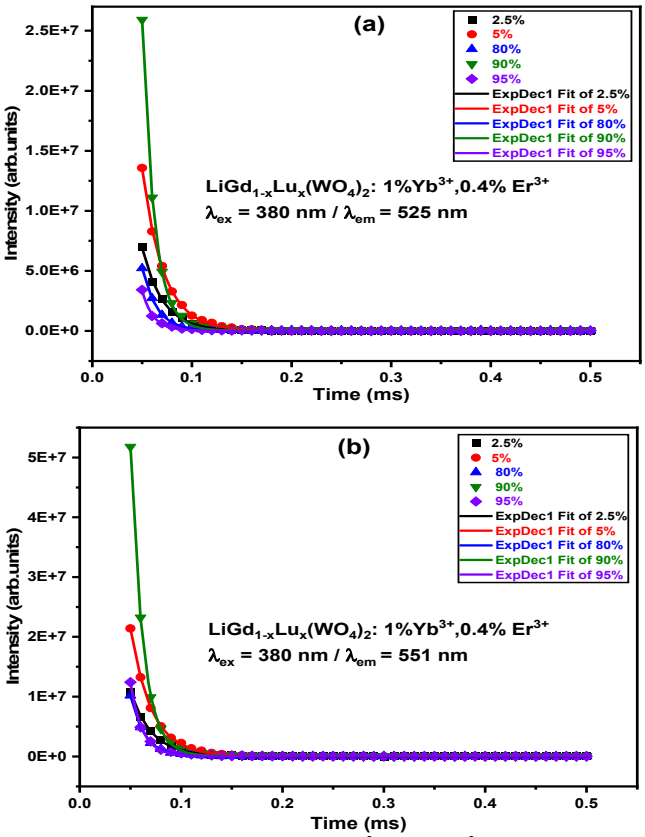

Figure 16. Decay curves of $LiGd_{1-x}Lu_x(WO_4)_2$: 1%Yb^{3+},0.4% Er^{3+} x=2.5%, 5%,80%, 90% and 95% monitored at (a) 525 nm and (b) 551 nm

The emission decay profiles were analyzed by fitting to a single-exponential function of the form:

$$I(t) = I_1 e^{-\left(\frac{t}{\tau_1}\right)} \tag{4}$$

Where *I(t)* denotes the emission intensity at time *t, I_1* is the initial intensity at *t = 0*, and τ_1 represents the corresponding decay lifetime.

The resulting decay lifetimes, along with the associated fitting parameters, are summarized in Table 6. The quality of the fits was satisfactory, as indicated by the goodness-of-fit parameters.

Table 6. Decay times of the $^2H_{11/2}$ and $^4S_{3/2}$ levels in $LiGd_{1-x}Lu_x(WO_4)_2$: 1%Yb^{3+},0.4%Er^{3+}

Lifetime (µs)	x = 2.5%	x = 5%	x = 80%	x = 90%	x = 95%
$^2H_{11/2}$	14.85	14.53	09.48	08.55	08.19
Reduced Chi-Sqr	1.22082E9	4.01423E9	2.1849E9	1.76239E10	1.34711E10
R-Square (COD)	0.99969	0.99974	0.99925	0.99976	0.99667
Adj. R-Square	0.99968	0.99973	0.99921	0.99975	0.99651
$^4S_{3/2}$	14.25	14.86	10.32	08.37	07.62
Reduced Chi-Sqr	9.65152E8	2.21119E9	7.45951E8	6.39374E9	1.44489E9
R-Square (COD)	0.9994	0.99965	0.99906	0.99965	0.99515
Adj. R-Square	0.99937	0.99963	0.99901	0.99963	0.99493

The decay curves show that the $^2H_{11/2}$ and $^4S_{3/2}$ emissions of Er^{3+} in $LiGd_{1-x}Lu_x(WO_4)_2$: 1%Yb^{3+},0.4%Er^{3+} are closely coupled and become progressively shorter-lived as Lu replaces Gd^{3+}. The PL decay behavior therefore indicates that Lu-rich compositions promote more efficient nonradiative or energy-transfer-assisted relaxation, reducing the persistence of green emission under 380 nm excitation [27-30]. There are two primary reasons why these values are less than those of the $LiLu(WO_4)_2$ co-doped Yb^{3+}/Er^{3+} examined in the reference [16]:

1. $LiLu(WO_4)_2$ co-doped with Yb^{3+}/Er^{3+} (24% and 4%), while Yb^{3+}/Er^{3+} (1% and 0.4%) is of lower grade.

2. Yb^{3+}/ Er^{3+} optimal ratio of 6 vs a ratio of 2.5 for $LiGd_{1-x}Lu_x(WO_4)_2$ compounds with x=2.5%, 5%,80%,90%, and 95%. [29].

CONCLUSIONS

In this study, a series of $LiGd_{1-x}Lu_x(WO_4)_2$: Yb^{3+}/Er^{3+} phosphors were successfully synthesized and characterized by XRD, FTIR, Raman spectroscopy, SEM, EDS, PLE and PL) to investigate their structural, vibrational, morphological, and optical properties. The progressive substitution of Gd^{3+} with Lu^{3+} ions, owing to their different ionic radii, induced significant in the crystal lattice. Raman analysis showed that increasing the Lu^{3+} concentration caused the Raman bands to shift toward higher wavenumbers together with a reduction in the full width at half maximum (FWHM), confirming a structural transition from tetragonal to monoclinic phase. The phosphors exhibited intense green up-conversion emissions in the 525-551 nm region, corresponding to the Er^{3+} ($^2H_{11/2}$ / $^4S_{3/2}$ to $^4I_{15/2}$) transitions, resulting from efficient energy transfer from Yb^{3+} sensitizers to Er^{3+} activators. Moreover, increasing the Lu^{3+} concentration produced a slight redshift in the emission bands, and reduced the fluorescence decay times Overall, these results demonstrate that $LiGd_{1-x}Lu_x(WO_4)_2$: Yb^{3+}/Er^{3+} phosphors exhibit up-conversion luminescence, highlighting their potential for advanced optical applications.

Acknowledgments

The authors would like to express their sincere gratitude to the General Directorate of Scientific Research and Technological Development (DGRSDT) to financial support and for facilitating the chemical and physical analyses.
Special appreciation is given to the researchers of the laboratory of Physical-Chemical Inorganic Materials and Their Applications (LPCMIA) at Saad Dahleb University Blida 1 for their valuable support and collaboration.
The authors also extend their thanks to CRTSE (Research Center in Semiconductor Technology for the Energetic) for carring out the optical examinations.

ORCID

Nesrine Naimi, https://orcid.org/0009-0005-0707-9641; **Brahim Rekik,** https://orcid.org/0000-0003-4944-3390
Imane Lanez, https://orcid.org/0000-0001-6758-9583; **Mourad Derbal,** https://orcid.org/0000-0001-9513-7736
Lyes Benharrat, https://orcid.org/0000-0002-6617-2222; **Zohour Bendaoud,** https://orcid.org/0009-0003-5780-3410

REFERENCES

[1] Enachi, O. Toma, and Ş. Georgescu, Journal of Luminescence, **231**, 117816 (2021). https://doi.org/10.1016/j.jlumin.2020.117816
[2] EF. Huerta, J. De Anda, I. Martínez-Merlin, U. Caldiño, and C. Falcony, Journal of Luminescence, **224**, 117271 (2020). https://doi.org/10.1016/j.jlumin.2020.117271
[3] G. Chen, H. Liu, H. Liang, G. Somesfalean, and Z. Zhang, The Journal of Physical Chemistry C, **112**, 12030-12036 (2008). https://doi.org/10.1021/jp804064g
[4] Li, D. Xu, Y. Zhang, H. Lin, S. Yang, Z. Chen, and Y. Shao, Journal of the American Ceramic Society, **99**, 1657-1663 (2016). https://doi.org/10.1111/jace.14141
[5] Wang, X. Chen, M. Xie, H. Lin, Y. Zhou, L. Liu, C. Li, and F. Zeng, Materials Research Bulletin, **94**, 435-441 (2017). https://doi.org/10.1016/j.materresbull.2017.06.038
[6] Shyichuk, S.S. Câmara, I.T. Weber, A.N.C. Neto, L.A. Nunes, S. Lis, R.L. Longo, and O.L. Malta, Journal of Luminescence, **170**, 560-570 (2016). https://doi.org/10.1016/j.jlumin.2015.07.005
[7] Mi, J. Wu, Y. Yang, B. Han, and J. Wei, Scientific reports, **6**, 22545 (2016). https://doi.org/10.1038/srep22545
[8] H. Shi, Y. Zhang, X. Wang, X. Ren, and S. Zhao, Optik, **258**, 168871 (2022). https://doi.org/10.1016/j.ijleo.2022.168871
[9] K.R. Kalimuthu, S.M. Babu, and V. Kalimuthu, Optical Materials, **102**, 109804 (2020). https://doi.org/10.1016/j.optmat.2020.109804
[10] Rekik, G. Alombert-Goget, A. Berthelot, O. Benamara, and K. Lebbou, Journal of Alloys and Compounds, **830**, 154165 (2020). https://doi.org/10.1016/j.jallcom.2020.154165
[11] X.Y. Huang, and G.F. Wang, J. Struct. Chem. **31**, 809–820 (2012).
[12] B. Rekik, M. Derbal, L. Guerbous, D. Ouadjaout, A. Nehari, E. Romeo, A. Brenier, and A.Yoshikawa, Optical Material, **33**, 1638-1642 (2011). https://doi.org/10.1016/j.optmat.2011.04.028
[13] W. ullah Khan, et al., RSC advances, **8**(71), 40693-40700 (2018). https://doi.org/10.1039/c8ra08374f
[14] J. Hanuza, M. Mączka, and JH. Van der Maas, Journal of molecular structure, **348**, 349-352 (1995). https://doi.org/10.1016/0022-2860(95)08660-N
[15] A. Demiaï, M. Derbal, L. Guerbous, and B. Rekik, Optical Materials, **65**, 137-141, (2017). https://doi.org/10.1016/j.optmat.2016.10.026
[16] X. Yun, J. Zhou, Y. Zhu, X. Li, S. Liu, C. Fang, M. Lv, and D. Xu, Journal of Physics and Chemistry of Solids, **163**, 110545 (2022). https://doi.org/10.1016/j.jpcs.2021.110545
[17] Li, et al., Journal of Materials Science: Materials in Electronics, **33**, 12259-12270 (2022). https://doi.org/10.1007/s10854-022-08185-x
[18] V.K. Pandey, V. Rai, V. Kumar, Kumar, and H.C. Swart, Sens Actuators B Chem. **209**, 352-8, (2015). https://doi.org/10.1016/j.snb.2014.11.126
[19] B. Rekik, M. Derbal, O. Benamara, and K. Lebbou, Journal of Crystal Growth, **405**, 11-15 (2014). https://doi.org/10.1016/j.jcrysgro.2014.07.032
[20] J. Hanuza, M. Mączka, and JH. Van der Mass, Journal of Solid State Chemistry, **117**, 177-188 (1995). https://doi.org/10.1006/jssc.1995.1261
[21] F. Bourgeois, Ph.D. Thesis, Lyon 1 University, 2000.
[22] Gallucci, Ph.D. Thesis, Lyon 1 University, 2000.

[23] M. Maczka, J. Hanuza, AF. Fuentes, and U. Amador, Journal of Raman Spectroscopy, **33**, 56-61 (2002). https://doi.org/10.1002/jrs.819
[24] R.F. Klevtsova, and S.V. Borisov, Kristallografiya, **14**, 610-612 (1969). https://doi.org/10.1007/10201585_18
[25] V.A. Efremov, and V.K. Trunov, Russ. J. Inorg. Chem. **19**, 272 (1974). https://doi.org/10.1088/0953-8984/8/44/013
[26] J. Hanuza, L. Macalik, M. Mączka, E.T.G. Lutz, and J.H. Van Der Maas, Journal of molecular structure, **511**, 85-106 (1999). https://doi.org/10.1016/S0022-2860(99)00148-9
[27] I. Lanez, B. Rekik, A. Kezzim, M. Derbal, T. Lanez, and K. Lebbou, Bull. Mater. Sci. **47**, 113 (2024). https://doi.org/10.1007/s12034-024-03194-4
[28] Li, J.G. Li, X. Li, and X. Sun, Ceramics International, **42**, 3268-3274 (2016). https://doi.org/10.1016/j.ceramint.2015.10.118
[29] W. Ahn, and Y.J. Kim, Optical Materials Express, **6**, 1099-1105 (2016). https://doi.org/10.1364/OME.6.001099
[30] R. Yun, J.He, L. Luo, X. Liu, Z. Nie, W. Zhao, and H. Wen, Ceramics International, (2021). https://doi.org/10.1016/j.ceramint.2021.02.180

СТРУКТУРНІ ТА ОПТИЧНІ ВЛАСТИВОСТІ LiGd1-xLux(WO4)2, СПІВЛЕГОВАНОГО Yb3+/Er3+, СИНТЕЗОВАНОГО МЕТОДОМ ТВЕРДОФІЛЬНОЇ РЕАКЦІЇ

Н. Наймі[1], Б. Рекік[1], І. Ланез[1], М. Дербаль[1], Л. Бенхаррат[2], З. Бендауд[1]

[1]Лабораторія LPCMIA, кафедра фізики, факультет природничих наук, Університет Саада Далеба Бліда 1, Бліда, BP 270 Soumaa Road, Бліда, Алжир

[2]Дослідницький центр напівпровідникових технологій для енергетики-CRTSE, 02 Bd. Dr. Frantz Fanon, B.P.140,7 Merveilles, 16038, м. Алжир, Алжир

Подвійні вольфраматні матеріали були ретельно вивчені та привернули значну увагу як твердотільні носії освітлення. Ці матеріали із загальною формулою $AB(WO_4)_2$ (A: лужний метал та B: тривалентний іон рідкісноземельного елемента) широко використовуються завдяки своїм чудовим оптичним властивостям. У цій роботі іони Gd^{3+} були частково заміщені іонами Lu^{3+} для синтезу сполук $LiGd_{1-x}Lu_x(WO_4)_2$ з метою вивчення структурної, коливальної та оптичної поведінки $LiGd_{1-x}Lu_x(WO_4)_2$, легованого іонами Yb^{3+} та Er^{3+}. Використовуючи твердофазну реакцію, для синтезу наших сполук були обрані різні концентрації Lu^{3+} (x=2,5%, 5%, 80%, 90% та 95%). Ці концентрації впливають на коливальні характеристики зв'язку W-O як через розширення зони, так і через зсув симетричної моди валентності (ν1). Щодо оптичних властивостей, у діапазоні 530-552 нм спостерігалося зелене апконверсійне випромінювання при збудженні 980 нм та апконверсійне випромінювання при збудженні 380 нм подвійного вольфрамату, легованого Yb^{3+} та Er^{3+}. Було порівняно та обговорено час життя рівнів $^2H_{11/2}$ та $^4S_{3/2}$, а також вплив заміщення Lu^{3+} на зелене випромінювання Er^{3+} у цих сполуках.

Ключові слова: *подвійний вольфрамат; легування Yb^{3+}/Er^{3+}; Up-конверсія; зелене випромінювання*